Optimal process design for the polygeneration of SNG, power and heat by hydrothermal gasification of waste biomass: Thermo-economic process modelling and integration

Martin Gassner[a], Frédéric Vogel[b], Georges Heyen[c], François Maréchal[a]

[a]Industrial Energy Systems Laboratory, Ecole Polytechnique Fédérale de Lausanne
CH – 1015 Lausanne, Switzerland
[b]Laboratory for Bioenergy and Catalysis, Paul Scherrer Institut, Villigen
CH – 5232 Villigen, Switzerland
[c]Laboratoire d'Analyse et Synthèse des Systèmes Chimiques, Université de Liège
B – 4000 Liège, Belgium

Abstract

This paper presents a process model for the polygeneration of Synthetic Natural Gas (SNG), power and heat by catalytic hydrothermal gasification of biomass and biomass wastes in supercritical water. Following a systematic process design methodology, thermodynamic property models and thermo-economic process models for hydrolysis, salt separation, gasification and the separation of CH_4, CO_2, H_2 and H_2O at high pressure are developed and validated with experimental data. Different strategies for an integrated separation of the crude product, heat supply and energy recovery are elaborated and assembled in a general superstructure. The influence of the process design on the performance is discussed for some representative scenarios that highlight the key aspects of the design. Based on this work, a thermo-economic optimisation will allow for determining the most promising options for the polygeneration of fuel and power depending on the available technology, catalyst lifetime, substrate type and plant scale.

Nomenclature

Abbreviations

EOS	Equation of state	
GT	Gas turbine	
MER	Minimum energy requirement	
$MILP$	Mixed integer linear programming	
$NGCC$	Natural gas combined cycle	
POX	Partial oxidation	
SNG	Synthetic natural gas	
$VL(E)$	Vapour-liquid (equilibrium)	
$WHSV$	Weight hourly space velocity	$kg_{biomass,daf}\,kg_{cat}^{-1}h^{-1}$

Greek letters

Δh^0	Lower heating value	$kJ\,kg^{-1}$
$\Delta \tilde{h}_r^{\,0}$	Standard heat of reaction	$kJ\,mol^{-1}$
Δk^0	Exergy value	$kJ\,kg^{-1}$
ΔT_{min}	Minimum approach temperature	K

ε	Energy efficiency	%
η	Exergy efficiency	%
Φ	Moisture	$\text{kg}_{H2O}\,\text{kg}_{tot}^{-1}$
ρ	Density	kg m^{-3}

Roman letters

A	Absorption factor	-
A	Area	m^2
C	Cost	\$ or \$ MWh^{-1}
c	Mass fraction	%
$\tilde{c}$	Molar fraction	%
d	Diameter	m
$\dot{E}$	Mechanical or electrical power, or exergy	kW
h	Specific enthalpy	kJ kg^{-1}
i_r	Interest rate	%
l	Length	m
$\dot{m}$	Mass flow	kg s^{-1}
$\tilde{m}$	Molecular weight	kg mol^{-1}
n	Expected plant lifetime	years
p	Pressure	bar
$\dot{Q}$	Heat flow	kW
$\tilde{R}$	Ideal gas constant	$\text{kJ K}^{-1}\,\text{mol}^{-1}$
r_{CH4}	Methane recovery	%
$\tilde{r}$	Molar ratio	-mol
T	Temperature	K
t_a	Yearly operating time	hours
U	Overall heat transfer coefficient	$\text{Wm}^{-2}\text{K}^{-1}$
V	Volume	m^3
y	Integer choices	-

Subscripts

be	break even
c	critical
cat	catalyst
daf	dry, ash-free
el	electric
GR	Grass roots (investment)
GR,d	depreciated grass roots
g	Gasification
lm	log-mean
M	Maintenance
max	maximum
min	minimum
OL	Operating labour
OP	Operation
pr	profitability
q	heat
r	reduced
s	Steam cycle
ss	Salt separation
th	thermal
tot	total
UT	utilities

Broader context

Biomass is a renewable, yet scarce resource since land is limited. Claimed by many as future feedstock to produce goods and provide energy, there is important concern about intensified farmland and forest exploitation and its inherent competition with food production.

Agricultural, industrial and municipal residues and wastes often hold a large share of a countrys unused non-fossil, carbonaceous energy resources and are not subject to the trilemma between food supply, energy supply and environmental protection. However, these potential resources are difficult to valorise since they are highly diluted and may contain harmful species for bacteria and catalysts, which greatly handicaps its biological or conventional thermochemical conversion to more versatile energy vectors than heat. Hydrothermal gasification allows for circumventing these obstacles by exploiting the advantageous properties of water at supercritical conditions.

Our research shows that the process design represents both a major challenge and opportunity for the successful development of energy- and cost-efficient technology. Using systematic methodology based on process modelling, integration and optimisation, it demonstrates how the design should adapt to constraints imposed by current technological limitations and feedstock impurities, and concludes that optimised configurations allow for saving up to 24% of Switzerlands greenhouse gas emissions with currently unused resources.

Superscripts

$^+$	Flows entering the system
$^-$	Flows leaving the system
^{0}	Standard conditions (i.e. 1 bar, 25°C)
^{l}	Liquid phase
^{v}	Vapour phase

1   Introduction

Conventional biomass conversion technologies for the production of fuel and power require relatively dry and clean feedstock and thus suffer from increasing competition for a relatively scarce resource. Hydrothermal gasification of biomass in supercritical water is a promising process alternative to produce synthetic natural gas (SNG) since it relaxes this requirement and grants access to a large range of low quality feedstocks such as wet lignocellulosic biomass and biomass wastes that are difficult to valorise by other means and thus relatively cheap.

In general, hydrothermal gasification is considered for the production of methane, hydrogen or combinations of these. Matsumura et al. [1], Kruse [2, 3], Elliott [4] and Peterson et al. [5] provide reviews on process fundamentals, chemistry, catalysis and principal technological developments and issues. Experimentally, Vogel et al. [6],[7] have demonstrated the production of methane from milled wood substrate in a batch reactor. During the subsequent development of a continuous process setup, the required salt separation at supercritical conditions has emerged as a main technological bottleneck. To understand this complex process step, Peterson et al. [8, 9] have performed visualisations of salt precipitation in a vertical tubular vessel, and Schubert et al. [10, 11] have conducted an extensive experimental study on the separation of different types of salt from supercritical water. Luterbacher et al. [12] have reported an overall process model and provided a first investigation of the process design and life cycle assessment for the hydrothermal production of SNG from wood and manure. Recently, the integration of hydrothermal gasification in fuel ethanol production and biorefinery systems to valorise black liquor and other residuals has received growing attention [13–15]. Moreover, microalgae are considered as a favourable feedstock since their production and gasification in a closed nutrient cycle would decouple energy crop based biofuels from food production [16, 17].

Among these previous studies which either discuss general process principles, present lab and pilot units or focus on detailed experimental investigations, Luterbacher et al. [12] have presented the only process design model that quantitatively takes energy integration and heat recovery into account. At the time of their developments, only limited insight into the salt separator design and the product separation was yet available. Energy integration has been performed on a scenario basis without optimisation, and the synergies between the reaction and separation subsystems through process integration have been disregarded.

The objective of this work is to systematically address the conceptual process design of hydrothermal gasification for the polygeneration of SNG, power and heat from wet lignocellulosic biomass and biomass wastes that are not accessible to the conventional technology [18]. This paper investigates process options and presents detailed thermo-economic models for the candidate technology that are validated and calibrated with experimental data. A general superstructure for integrated product separation, power recovery and heat supply is established and the benefits of process integration are explored. These developments prepare the detailed thermo-economic optimisation of the process design that is addressed in an associated paper [19].

2 Methodology

2.1 Conceptual process design

This work follows a previously developed methodology for the conceptual design of thermochemical production of fuels from biomass [20]. Similar to a classical design procedure, the analysis of raw material characteristics, product specifications and feasible production pathways allows for identifying suitable technology for the process unit operations and energy recovery that are assembled in a process superstructure. A decomposition-based modelling approach is then adopted to systematically develop candidate flowsheets. First, the thermochemical conversion and the energy requirements of the process units are computed in energy-flow models that are developed in flowsheeting software [21]. The combined mass- and energy integration is then performed by mixed integer linear programming (MILP), in which both the material flows defined by the superstructure and the heat cascade – that represents the heat exchanger network – act as constraints [22]. Considering waste and intermediate product streams as fuel to supply the required heat, the combined SNG, heat and power production is optimised with respect to operating cost. For the so-determined flowsheet, all the equipment is rated with design heuristics and laboratory and pilot plant data to meet the thermodynamic design target. This allows for evaluating the economics and the thermo-economic optimisation of the process with multi-objective optimisation techniques.

2.2 Performance indicators

Throughout the analysis, the thermodynamic performance of process flowsheets is discussed regarding the conversion efficiencies of the products, i.e. SNG (1), electricity (2) and heat (3):

$$\varepsilon_{SNG} = \frac{\Delta h^0_{SNG} \dot{m}^-_{SNG}}{\Delta h^0_{biomass} \dot{m}^+_{biomass,daf}} \tag{1}$$

$$\varepsilon_{el} = \frac{\dot{E}^-}{\Delta h^0_{biomass} \dot{m}^+_{biomass,daf}} \tag{2}$$

$$\varepsilon_{th} = \frac{\dot{Q}^-}{\Delta h^0_{biomass} \dot{m}^+_{biomass,daf}} \tag{3}$$

and the overall energy ε, exergy η and 'chemical' ε_{chem} efficiencies defined as, respectively:

$$\varepsilon = \frac{\Delta h^0_{SNG} \dot{m}^-_{SNG} + \dot{E}^- + \dot{Q}^-}{\Delta h^0_{biomass} \dot{m}^+_{biomass,daf} + \dot{E}^+} \tag{4}$$

4
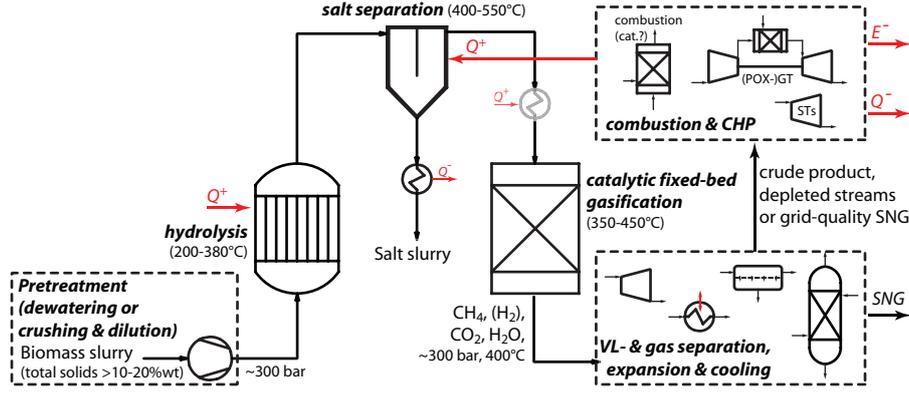
Figure 1: Conceptual process flow diagram for hydrothermal gasification in supercritical water

$$\eta = \frac{\Delta k^0_{SNG} \dot{m}^-_{SNG} + \dot{E}^- + \dot{E_q}^-}{\Delta k^0_{biomass} \dot{m}^+_{biomass,daf} + \dot{E}^+} \tag{5}$$

$$\varepsilon_{chem} = \frac{\Delta h^0_{SNG} \dot{m}^-_{SNG} + \frac{1}{\eta_{NGCC}} \frac{\Delta h^0_{SNG}}{\Delta k^0_{SNG}} \left(\dot{E}^- + \frac{\dot{E_q}^-}{\eta_{HP}} \right)}{\Delta h^0_{biomass} \dot{m}^+_{biomass,daf}} \tag{6}$$

In these definitions, Δh^0 and Δk^0 designate the dry lower heating and exergy values, and $\dot{m}$ the mass flow of SNG and biomass. $\dot{E}$, $\dot{Q}$ and $\dot{E}_q$ represent electrical power, heat and the exergy of heat. For all hydrocarbon substrates and intermediate macromolecular groups without a strict thermodynamic definition of their enthalpy of formation and entropy, Δh^0 and Δk^0 are thereby determined with the correlations of Boie [23] and Szargut and Styrylska [24]. The superscripts $^-$ and $^+$ refer to produced and consumed services, respectively. In Eqns. (4) and (5), only the positive value of $\dot{E}$ occurs either in the numerator or denominator, while Eqns. (2) and (6) assess net electricity consumption by a negative value of $\dot{E}^-$. The production of heat is only useful if it is provided at a sufficient temperature level to be used locally and is considered zero otherwise.

The overall energy and exergy indicators ε and η provide a strictly physical measure of the energy conversion and its quality degradation. Yet, they do not satisfactorily assess the value of the products with respect to the efficiency of their further conversion into final energy services and competing technologies [14]. The technical value of the cogeneration products are therefore assessed in terms of the fuel-equivalent efficiency ε_{chem}, in which the net electricity balance is substituted by the equivalent amount of (synthetic) natural gas that is consumed or saved in reference technology. Aiming at a consistent weighting with efficient state-of-the-art technology, electricity is represented by a natural gas combined cycle (NGCC), and heat by electricity-driven heat pumps (HP), both with an exergy efficiency of $\eta_{NGCC} = \eta_{HP} = 55\%$. This corresponds to an energy efficiency of $\varepsilon_{NGCC} = 57\%$ and performance coefficients of 3.1 and 1.6 for electricity- and gas driven heat pumps in a district heating network with supply and return temperatures of 110 and 70°C, respectively. From an energy systems perspective, this substitution is letigimate and leads to a consistent and technologically reasonable appraisal of the different energy vectors [25].

Following the approach of Turton et al. [26], the economic performance assessment is based on several indicators considering investment and operating costs, which are detailed in the economic model of Section 6.

3 Process analysis

3.1 Thermodynamic considerations

The conversion of biomass into methane and carbon dioxide is based on the conceptual overall net reaction, which can be written for a typical composition of lignocellulosic matter:

$$CH_{1.35}O_{0.63} + 0.3475\,H_2O \rightarrow 0.51125\,CH_4 + 0.48875\,CO_2, \quad \Delta\tilde{h}_r^{\;0} = \text{-10.5 kJmol}^{-1}_{\text{biomass}} \tag{7}$$
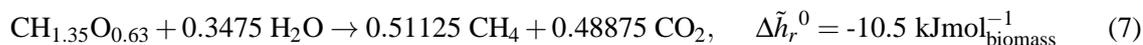
Technically, the conversion requires a heterogeneous catalyst and is thus impossible to perform directly with the solid biomass feed since the big macromolecules cannot access the active sites on the catalyst. The most envisaged route is thus to first decompose the solid feedstock by conventional gasification and then catalytically synthesise the obtained H_2/CO-rich gas into CH_4 and CO_2 [18]. The conversion of Equation (7) therefore splits up in an endothermal gasification step at high temperature (typically above 800°C) and an exothermal synthesis step at 300-400°C at which CH_4 is thermodynamically favoured. This limits the product yield since a considerable part of the energy content of the feed is required to form intermediate H_2/CO and is then converted into excess heat in its highly exothermal methanation [27].

Contrary to this two-step layout, the hydrothermal route omits the endothermal step at high temperature and targets a direct conversion of diluted biomass at 300-400°C into CH_4 and CO_2. Instead of forming an intermediate gas, the biomass is hydrolysed and gasified in a supercritical aqueous environment at around 300 bar, which allows for an efficient contact with the catalyst [7]. The fluid processing thereby requires a feed in the form of a pumpable slurry with typical total solid contents of 20-50%wt depending on the type of substrate [6, 7]. Although this makes the process suitable for wet biomass since the heat requirement up to the gasification temperature is reduced by the high pressure and drying is not required, the design must take care of the high amount of water that accompanies the reacting species throughout the process. As this represents the major share of the heat transfer requirements, the overall performance gets sensitive to the energy integration of the plant.

3.2 Technical process layout

Depending on the moisture and type of biomass that is processed, the first step in the conceptual process flow diagram of Figure 1 is to control its pumpability by mechanical dewatering and/or grinding and diluting the feed. The slurry is then compressed to around 300 bar and heated close to critical conditions at 350-380°C. During this step, the biomass is hydrolysed into smaller molecules that can access to catalytic sites [7]. When being heated above the pseudo-critical point[2], the fluid density decreases significantly, and with it the solubility of inorganics that are present in the feedstock. They will thus precipitate as salts and risk to plug the equipment and deactivate the catalyst if they are not efficiently removed. To do so, the subcritical slurry is injected through a dip-tube into a heated vessel to reach supercritical conditions, at which the precipitating salts are separated by gravitation in an equipment similar to a cyclone. The main flow reverses and leaves the vessel at the top [8–11]. The supercritical hydrolysate then passes through a fixed bed of a nickel- or ruthenium-based catalyst, which converts, at ideal conditions, more than 99.9% of the organic matter into a near-equilibrium mixture of CH_4, CO_2, some H_2 and only traces of CO [6]. If the temperature risks to drop significantly below 400°C due to the endothermic reactions, preheating of the feed or an external heating of the reactor tubes is thereby required.

In order to inject the produced methane at the required purity of 96%mol into the natural gas grid [28], it must be separated from water, carbon dioxide and possibly hydrogen. For a typical lignocellulosic feedstock of Equation (7) diluted to 20%wt total solids, the crude product thereby contains approximately 84%mol of H_2O and 8%mol of each CH_4 and CO_2 in a supercritical mixture at 300-400°C and around 300 bar. The design of the product separation should yet not only consider the grid quality specifications for SNG, but also the recovery of the exergy potential of the crude gas and the supply of required heat for

---

[2]i.e. the temperature at which the specific heat capacity reaches its maximum value on the isobar

the plant. For a similar separation problem in conventional SNG production, the tight integration of the reactive and separation systems have generated process intensification effects that can also be expected for a hydrothermal plant [29].

4 Process modelling

4.1 Thermodynamic property models

Due to the targeted biomass conversion in supercritical water, the process design is confronted with rather particular thermodynamic conditions. With the bulk substance H_2O present at reduced pressures $p_r = p/p_c$ up to 1.4 and temperatures $T_r = T/T_c$ in the range of 0.5 to 1.1, the operations are carried out in very different regions of the phase diagram. In hydrolysis, a suspended organic solid is decomposed at subcritical temperature into a large range of organic compounds. The mixture is then heated above the pseudo-critial point, where the inorganic fraction precipitates and needs to be removed in the salt separator. Gasification is carried out at supercritical conditions, and the crude product expanded and separated somewhere in the gas- and two-phase regions at different compositions.

In order to ensure a reliable process design, several requirements are to be met by the thermodynamic model. The bulk of the accompanying water causes the enthalpy-temperature profiles of the hot and cold streams to be non-linear and very tight. A change in temperature of a few degrees may considerably disturb the pinch point and thus the performance of the process. The prediction of these profiles must therefore be valid and consistent over the entire range of the process operating conditions. A second critical requirement is the accurate evaluation of the vapour-liquid equilibrium (VLE) in the bulk separation, which needs to be able to reproduce the considerable non-idealities due to the polarity of H_2O and the fact that the conditions in the separation may approach the critical point of CO_2 at 31°C and 74 bar. Finally, the process design methodology imposes a thermodynamic model that is computationally robust in order to evaluate the process model at very different conditions during the optimisation.

Although simple linear models like Henry's law are very convenient at low pressures, they fail at higher pressures where the assumption of infinite dilution does not hold anymore. Approaches based on a general equation of state (EOS), as for example the classic ones by Peng and Robinson [30] or Lee and Kesler [31], are better suited for the high pressure domain, but lack accuracy for VLE equilibria in the present mixture. Peng-Robinson is a Van der Waals type EOS and thus suitable to represent moderate non-idealities, but has poor accuracy for polar mixtures. The Lee-Kesler EOS is reasonable for general purposes, but not accurate enough to represent the phase equilibrium of the H_2O-CO_2-CH_4 system. For this reason, Duan et al. [32, 33] have developed and parametrised a modified form of the Lee-Kesler equation with experimental pVT and binary solvus data over a very large temperature and pressure range (0(50-1000°C, 0-8000(1000) bar). Although promising for our application, the evaluation of this equation at the prevailing process conditions has revealed some major weaknesses that prevent its direct application.

A hybrid approach has finally proved suitable [14]. Above 250°C, the homogeneous EOS of Duan et al. [32, 33], generalised by Esser and Heyen [34] to more compounds than the ternary H_2O-CO_2-CH_4 mixture, proves valid for VLE calculations and assures coherency in the critical zone. Below 250°C, however, the EOS looses both accuracy and robustness and a heterogeneous solubility model is used instead. For this purpose, we have extended the binary models for the H_2O-CO_2 and H_2O-CH_4 systems proposed by Duan and Sun [35] and Duan and Mao [36] to the ternary mixture by regressing activity coefficients that account for the interactions between CO_2 and CH_4 that have recently been reported in the ternary data of Qin et al. [37]. With this correction, the ternary model reaches the precision of the binary model [14]. Throughout the process, enthalpy is consistently evaluated with the original Lee-Kesler equation since the Duan EOS shows severe deviations from reliable data for pure water.

7
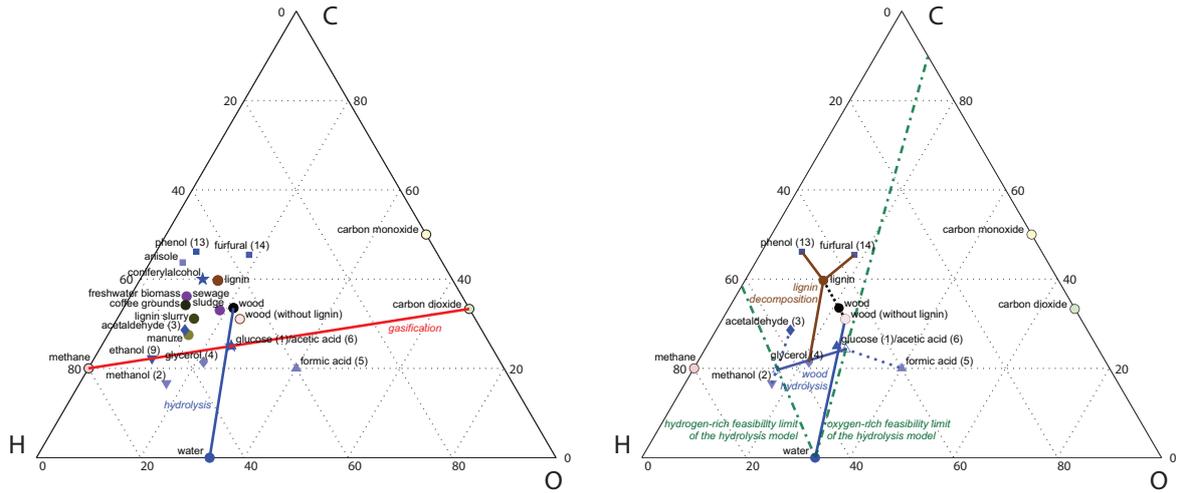
(a) Potential feedstocks, main intermediate hydrolysis prod- (b) Decomposition of wood and feasibility range of the model
ucts, overall reactions and final products

Figure 2: Molar ternary diagram of the hydrolysis model. Numbers in parenthesis indicate the quantitative rank of
the substances detected in the liquefaction experiment by Waldner and Vogel [7]

4.2 Hydrolysis

The breakdown of lignocellulosic biomass into its macromolecular components cellulose, hemicellulose
and lignin and their hydrolysis into a wide spectrum of smaller molecules follows multiple complex
reaction paths that are impractical to detail in a conceptual process design model. In a liquefaction ex-
periment at 303°C and 122 bar in water and the presence of a nickel catalyst, Waldner and Vogel [7]
have identified the main intermediate species in the decomposition and developed a simplified reaction
network. In the model of Luterbacher et al. [12], these findings have been used to adjust an approxi-
mate hydrolysate composition based on a few model species for wood and manure. They have thereby
followed a procedure by hand, which is not generalisable since the decomposition into model species is
underdetermined and even infeasible for certain potentially interesting substrates.

In order to generalise the scope of the process model, a simple and systematic decomposition scheme
that is feasible for a wide range of substances has been developed. The model species are thereby
chosen among the principal experimentally observed substances that are located in the ternary diagram
of Figure 2(a). Following the considerations of Waldner and Vogel [7], different reaction pathways
for lignin and (hemi-)cellulosic parts are expected. The biomass is thus first divided into these two
macromolecular groups:

$$biomass \rightarrow (hemi-)cellulose + lignin$$

$$\text{i.e.: } CH_{\tilde{r}_{bm,H}}O_{\tilde{r}_{bm,O}} \rightarrow (1 - \tilde{c}_{lignin})\, CH_{\tilde{r}_{cel,H}}O_{\tilde{r}_{cel,O}} \tag{8}$$

$$+ \tilde{c}_{lignin}\, CH_{\tilde{r}_{lig,H}}O_{\tilde{r}_{lig,O}}$$
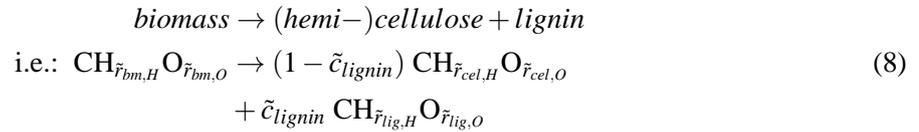
$$\text{with: } \quad \tilde{r}_{cel,H} = \frac{\tilde{r}_{bm,H} - \tilde{r}_{lig,H}}{1 - \tilde{c}_{lignin}} + \tilde{r}_{lig,H} \tag{9}$$

$$\tilde{r}_{cel,O} = \frac{\tilde{r}_{bm,O} - \tilde{r}_{lig,O}}{1 - \tilde{c}_{lignin}} + \tilde{r}_{lig,O} \tag{10}$$

$$\tilde{c}_{lignin} = \frac{\tilde{m}_{biomass}}{\tilde{m}_{lignin}}\, c_{lignin} \tag{11}$$

in which $\tilde{r}$ represents molar ratios, and c_{lignin} and $\tilde{c}_{lignin}$ the mass and molar fraction of lignin in the
feedstock, respectively.

During hydrolysis, the (hemi-)cellulosic parts are degraded to glucose and further via 5-hydroxymethyl
furfural to carboxylic acids, aldehydes and alcohols [7]. Among the experimentally identified substances,

the most abundant have been chosen as model species, and the decomposition of the hemo-cellulosic group is represented by:

$$(hemi-)cellulose + water$$
$$\rightarrow acetic\ acid + formic\ acid$$
$$+ acetaldehyde + methanol$$
$$\text{i.e.: } CH_{\tilde{r}_{cel,H}}O_{\tilde{r}_{cel,O}} + \tilde{r}_{H2O}\ H_2O \tag{12}$$
$$\rightarrow \tilde{r}_{acetic\ acid}\ CH_3COOH + \tilde{r}_{formic\ acid}\ HCOOH$$
$$+ \tilde{r}_{acetaldehyde}\ CH_3CHO + \tilde{r}_{methanol}\ CH_3OH$$
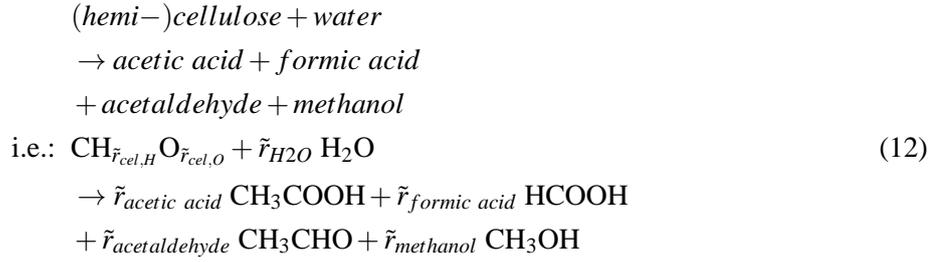
Lignin is typically converted to phenolic and other aromatic compounds and then further to the same final products as cellulose and hemicellulose. In order to represent the more carbon-rich lignin-derivatives, phenol and furfural are included as model species, and the lignin decomposition is balanced with the abundant glycerol as indicated by the brown lines on Figure 2(b):

$$lignin \rightarrow phenol + furfural + glycerol$$
$$\text{i.e.: } CH_{\tilde{r}_{lig,H}}O_{\tilde{r}_{lig,O}} \rightarrow \tilde{r}_{phenol}\ C_6H_6O \tag{13}$$
$$+ \tilde{r}_{furfural}\ C_5H_4O_2 + \tilde{r}_{glycerol}\ C_3H_8O_3$$
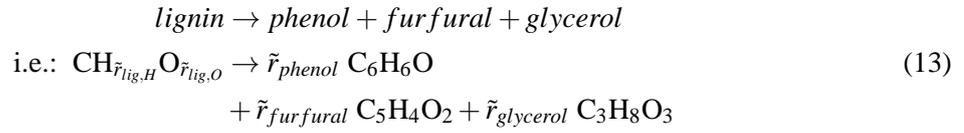
In addition to the three atomic balances of C, H and O, Equations (8-11) require the lignin-characteristics r_{lignin}, $\tilde{r}_{lig,H}$ and $\tilde{r}_{lig,O}$ of the substrate, while two more specifications are needed to determine the stoichiometric coefficients of the hydrolysis reaction (12). For this purpose, the experimental data [7] are used to assess typical ratios between the most abundant intermediates:

$$\tilde{r}_{acids} = \frac{\tilde{r}_{acetic\ acid}}{\tilde{r}_{formic\ acid}} = \frac{\tilde{c}_{acetic\ acid}}{\tilde{c}_{formic\ acid}} = \frac{\tilde{c}_{acetic\ acid+glucose}}{\tilde{c}_{formic\ acid}} \tag{14}$$

$$\tilde{r}_{alcohol/aldehyde} = \frac{\tilde{r}_{methanol}}{\tilde{r}_{acetaldehyde}} = \frac{\tilde{c}_{methanol}}{\tilde{c}_{acetaldehyde}} \tag{15}$$

where glucose as principal decomposition product is included in the share of acetic acid due to their identical molar composition. On the ternary diagram of Figure 2(b), these ratios fix the intermediate points on the blue-dotted lines and determine the amount of water that is consumed during hydrolysis.

With the data of Table 1, Eqns. (8) to (13) write for the typical biomass composition of Equation (7) as, respectively:

$$CH_{1.35}O_{0.63} \rightarrow 0.658\ CH_{1.46}O_{0.76} + 0.342\ CH_{1.14}O_{0.38} \tag{16}$$

$$CH_{1.46}O_{0.76} + 0.329\ H_2O \rightarrow 0.402\ CH_3COOH$$
$$+ 0.105\ HCOOH + 0.016\ CH_3CHO$$
$$+ 0.059\ CH_3OH, \quad \Delta\tilde{h}_r{}^0 = 7.7\ kJmol^{-1}_{CH_{1.46}O_{0.76}} \tag{17}$$
$$CH_{1.14}O_{0.38} \rightarrow 0.072\ C_6H_6O + 0.086\ C_5H_4O_2$$
$$+ 0.045\ C_3H_8O_3, \quad \Delta\tilde{h}_r{}^0 = 115\ kJmol^{-1}_{CH_{1.14}O_{0.38}} \tag{18}$$
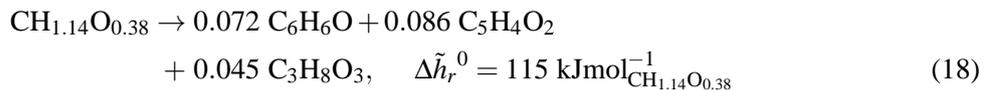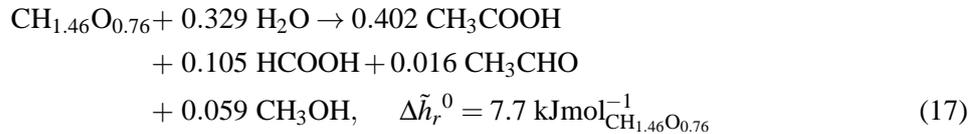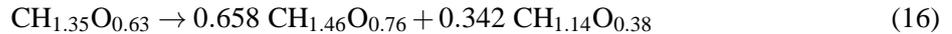
In this way, the decomposition model includes the main families of the observed species and can be applied to a broad range of potential substrates. According to the conservatively estimated hydrolysis kinetics [12], these reactions are assumed to take place between approximately 250 and 350°C with a peak at 320°C.

4.3 Salt separation

The currently envisaged design of the salt separator of Figure 3 consists in a vertical, tubular vessel in which the hydrolysate is injected through a dip tube [8–11]. By externally heating the vessel, the

Table 1: Hydrolysis model parameters based on lignin composition from ECN [38] and hydrolysis data of Waldner and Vogel [7]

Parameter		Unit	Value
Biomass and lignin composition:			
ligin fraction in biomass	c_{lignin}	%wt$_{daf}$	28
H/C-ratio of lignin	$\tilde{r}_{lig,H}$	-mol$_{daf}$	1.14
O/C-ratio of lignin	$\tilde{r}_{lig,O}$	-mol$_{daf}$	0.38
Hydrolysate composition:			
acids-ratio	$\tilde{r}_{acids}$	-mol$_{daf}$	3.82
alcohol/aldehyde-ratio	$\tilde{r}_{alcohol/aldehyde}$	-mol$_{daf}$	3.57

Table 2: Salt separator heat transfer model reconciliation using data from Schubert et al. [10]

Zone	Exchanging fluids		Flow pattern	l_z	$d_{i,z}$	$d_{o,z}$	$d_{lm,z}$	U_z[a]	Conf.[b]
					[mm]			[Wm^{-2}K^{-1}]	[%]
Dip tube	inner dip tube	exit stream	countercurrent	212	1.5	3.0	2.16	4'190	15.0
	exit stream	heating medium	co-/counterc.[c]	212	12	50	26.6	477	13.0
Flow reversal	mixed fluid	heating medium	co-/counterc.[c]	120	12	50	26.6	268	10.2
Salt brine layer	salt brine	heating medium	co-/counterc.[c]	120	12	50	26.6	13	25.0

[a] U is dependent on d and thus not valid for other diameters than the ones reported here

[b] 95%-confidence interval for U_z assuming a normal distribution

[c] Experiments have been conducted with an electric heating block at constant temperature and do thus not correspond to a flow pattern. For the process design, the reconciled U can be used for both co- and countercurrent modes

mixture passes its pseudo-critical point, at which the solubility of the salts decreases and causes them to precipitate in a salt brine that is withdrawn at the vessel bottom. As the fluid temperature increases, the bulk flow reverses and leaves the vessel at the top. In their model, Luterbacher et al. [12] have not considered the detailed equipment design of the salt separator and assumed a linear hT-profile from inlet to outlet to represent the heat exchange requirement with a minimum approach temperature contribution $\Delta T_{min}/2$ of only $4°C$. From an engineering perspective, this is most likely a too optimistic assumption for the heat transfer at the technological bottleneck and pinch point of the process, and a better definition of the heat transfer requirement that guarantees the feasibility of the heat exchanger design is needed.

Based on the experimentally measured temperature profiles along the vessel axis [10], a technologically sound hT-profile representation of the heat requirement during salt separation is proposed here. As shown in Figure 3, the heat exchange is divided into several zones with different flow patterns and heat transfer characteristics. In the dip tube zone, heat is exchanged internally between the entering fluid and the main exit stream, and through the outer wall between the exit stream and the external heating medium. In the flow reversal zone, heat is delivered from the external heating medium to the entire mixture, whereas only the precipitated salt slurry is affected in the salt brine layer zone at the bottom of the vessel. Using the experimental data for different operating conditions of the salt separator, overall heat transfer coefficients U_z for these zones z are reconciled with the general law of the form:

$$\dot{Q}_z = A_z U_z \Delta T_{lm,z} = \pi l_z d_{lm,z} U_z \Delta T_{lm,z}, \quad d_{lm,z} = \frac{d_{o,z} - d_{i,z}}{\ln(d_{o,z}/d_{i,z})} \quad (19)$$

where $\dot{Q}_z$ is the exchanged heat, A_z the area, l_z the section length, $d_{i,z}$ and $d_{o,z}$ the inner and outer diameter of the heat exchanger tube, respectively, and $\Delta T_{lm,z}$ the log-mean temperature difference in the heat exchange zone z. As the heat transfer is dependent on the flow regime (i.e. Reynolds and Prandtl numbers), the reconciled values for U shown in Table 2 are not valid for diameters and flowrates different from the ones in the experimental setup. In this regard, the values represent minimum design targets to achieve the required duty. This should be possible if the geometry of the tubes' cross sections is preserved and scaling is done by varying only their number and length, which has been considered in this study.

Equation (19) used with distinct transfer coefficients U_z for each zone represents the basis of a thermo-economic model for the salt separator, in which the hT-profiles are related to the required zone length
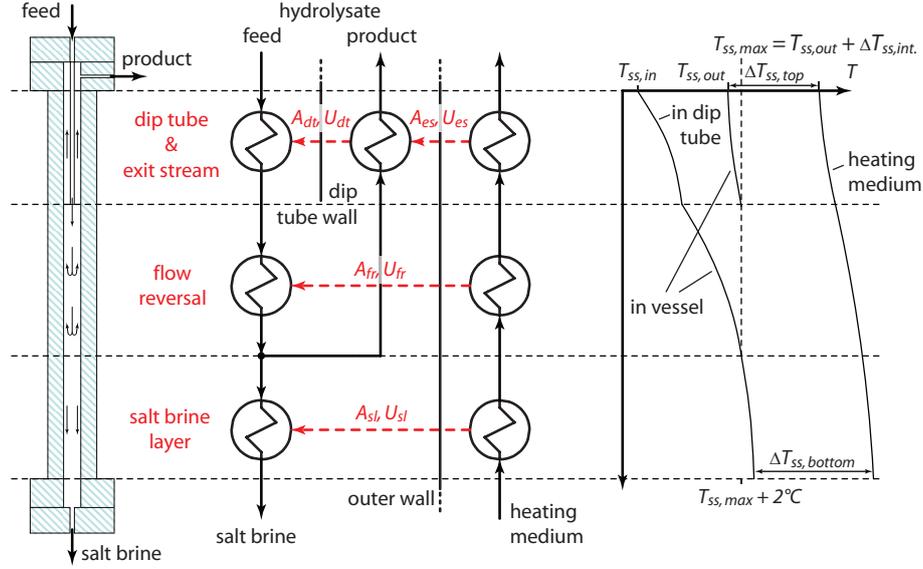
Figure 3: Schematic of the salt separator and its heat transfer model representation

of a separator tube with diameters of Table 2. In order to increase the total flowrate during scale-up, the vessel could be designed as a bundle of vertically arranged separator tubes including each a dip tube. The required area of this shell-and-tube like heat exchanger is then determined by specifying the targeted inlet and outlet temperatures of the hydrolysate and the heating medium. This approach complies with the proposed methodology that considers the thermodynamic requirements as a target for the equipment design [20].

In order to assess the catalyst poisoning in the gasifier by residual sulphur, the salt concentration at the separator outlet is estimated with the solubility correlation of Leusbrock et al. [39] for Na_2SO_4 in supercritical water:

$$\ln\left(\frac{\tilde{c}_{Na2SO4}}{\tilde{m}}\right) = \frac{-31.337}{\tilde{R}T_{ss}} - \frac{0.16661}{\tilde{R}} + 7.132\,\ln\left(\frac{\rho_{ss}}{\tilde{m}}\right) \qquad (20)$$

in which $\tilde{c}_{Na2SO4}$ is the molar fraction of diluted salt, $\tilde{R}$ the ideal gas constant, and T_{ss}, ρ_{ss} and $\tilde{m}$ the temperature, density and molar weight of the saturated fluid at the separation temperature, respectively. Due to the lack of data for organic mixtures at these conditions, the correlation with respect to the fluid's molar density $\rho_{ss}/\tilde{m}$ is applied without modification. At the same temperature and pressure, this results in an increased salt solubility due to the increased density of the organic mixture compared to pure water. As the separation does not occur at the hottest point[8–11], the arithmetic average of the molar density and temperature $\rho_{ss} = (\rho_{ss,max} + \rho_{ss,out})/2$ and $T_{ss} = (T_{ss,max} + T_{ss,out})/2$ between the flow reversal and the top exit are considered in the correlation. For the organic loss in the salt brine, a conservative value of 10% of the salt separator feed is assumed based on the acquired experience [10, 11].

4.4 Gasification

Originally demonstrated in a batch reactor, the ongoing development of a continuous process envisages a downflow fixed bed design for the slightly endothermal gasification reaction [6, 10, 40]. The experimental results indicate that equilibrium conversion to CH_4, CO_2, residual H_2 and traces of CO can be reached with a weight hourly space velocity (WHSV) of no more than 2 $kg_{biomass,daf}kg_{cat}^{-1}h^{-1}$ for gasification temperatures around 400°C. If the temperature drop due to the endothermicity is too high, heating the feed after the salt separator or external heating of the reactor tubes might be envisaged to assure a good conversion. Catalyst deactivation is estimated assuming that 1 mol of sulphur poisons 1 mol of ruthenium, which is dispersed on the support to 100% and represents $q_{Ru,cat}$ =2%wt of the total dry
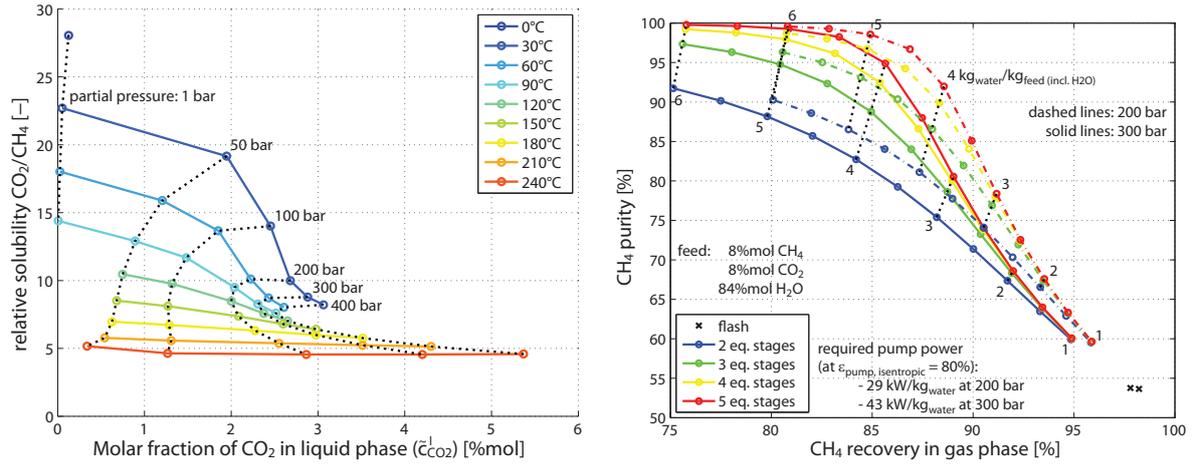
(a) Relative solubilities of CO_2 and CH_4 in their binary mixture with water (data according to Duan and Sun [35], Duan and Mao [36])

(b) Performance of CO_2/CH_4-separation in an absorption column with water

Figure 4: Characteristics of the separation of CO_2 and CH_4 with water under high pressure

catalyst mass [10]. Accordingly, the catalyst replacement rate $\dot{m}_{cat}$ [kg s^{-1}] is calcuated as:

$$\dot{m}_{cat} = \frac{\tilde{c}_{Na2SO4}}{\tilde{m}_{ss,out}} \frac{\tilde{m}_{Ru}}{c_{Ru,cat}} \dot{m}_{ss,out} \tag{21}$$

in which the first fraction represents the salt concentration [mol kg^{-1}] of Eq. (20), $\tilde{m}_{Ru}$ the molecular weight of ruthenium [kg mol^{-1}] and $\dot{m}_{ss,out}$ the flowrate [kg s^{-1}] of the substrate.

4.5 Integrated product separation, heat supply and mechanical energy recovery

With the typical feed composition of Equation (7) diluted to 20%wt total solids, the crude product from gasification contains more than 80%mol H_2O, approximately equal amounts of CH_4 and CO_2 and some marginal H_2 and CO. Due to the supercritical conditions, its upgrade and expansion to grid conditions potentially allows for recovering mechanical energy, which however competes with the supply of thermal energy required for hydrolysis and salt separation. Another important aspect of the separation system design is the quality of the depleted stream, which may be used to supply the required heat and thus relax the need for a high level of methane recovery in the separation. The given boundary conditions thereby suggest two different separation strategies. Apart from conventional absorptive separation at grid pressure with a dedicated physical solvent followed by a membrane stage to remove residual hydrogen [18], the better solubility of CO_2 compared to CH_4 in water may become technically relevant at the prevailing process pressure. As shown by the absolute and relative solubilities of CO_2 towards CH_4 in their binary mixtures with water depicted in Figure 4(a), the relative solubility deteriorates with increasing pressure, and a trade-off between selectivity and absolute solubility might occur. In any case, the separation is best at low temperature, and additional water is required for absorbing the amount of CO_2 required to reach grid quality natural gas. The expected separation performance for a typical crude composition as calculated with the developed thermodynamic model is shown in Figure 4(b). Compared to a simple flash stage where only a marginal separation occurs, several equilibrium stages and additional water allows for purifying the crude product up to the required 96%mol methane. The increase in purity is thereby rather steep at low rates of additional water, but flattens out at higher rates, which has a considerable impact on the pumping power required to attain high purity. As expected from the trade-off observed in Figure 4(a), decreasing the absolute pressure increases the methane recovery due to the change in relative solubility and only marginally affects the attained purity.

In order to recover mechanical energy from the crude product at high pressure, the separated vapour phase – or the entire supercritical bulk phase, if no high pressure separation is applied – may be expanded
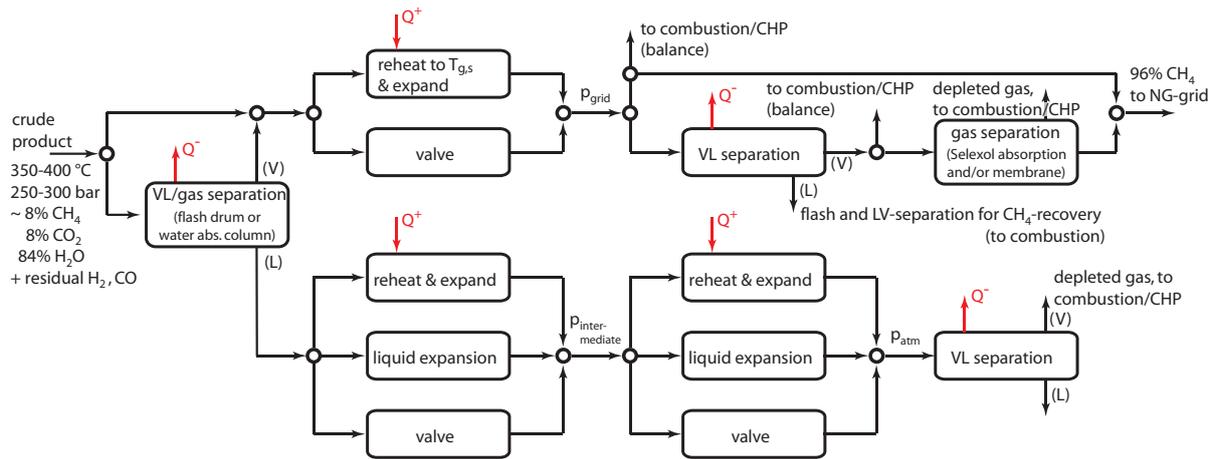
Figure 5: Superstructure including all possibilities for integrated product separation, heat supply and mechanical energy recovery

through turbines. It might thereby be advantageous or even necessary to preheat the stream, which increases the thermal efficiency of the mechanical power recovery and prevents an expansion too far into the two-phase region. Compared to an adiabatic expansion through valves, this causes less heat to be available from the crude product stream since energy is withdrawn at high temperature, and can lead to suboptimality if done above the process pinch. For the liquid phase obtained from the separation at high pressure, power can be recovered by liquid expanders. This technology is currently being commercialised in natural gas liquefaction plants, where it also copes with expansions that partially result in a vapour phase [41]. As an alternative, the liquid phase could also be reheated and expanded into the vapour domain, which would allow for extracting more mechanical energy from the available potential, but also requires a considerable amount of heat to be supplied.

A general superstructure with all these options for integrated product separation, heat supply and mechanical energy recovery is outlined in Figure 5. If the product is not upgraded to grid quality at high pressure, the vapour-liquid (VL) and gas separations need to be carried out after the expansion of the crude product. In this case, the same technologies and models as for the more conventional SNG production by methanation of producer gas can be applied [18]. For bulk gas separation at grid pressure, a Selexol column seems appropriate. The combination of both high pressure and grid pressure separation is also conceivable. In order to reduce the amount of required additional water and thus pump power, the gas could only be pre-separated at high pressure and a single polymeric membrane stage at grid pressure could be used. For a good separation performance of the latter, the partial pressure of CO_2 in the membrane feed should however not exceed 10-20 bar to avoid a decrease in selectivity due to plasticisation [42].

5 Process integration

As detailed in the methodology, the energy integration of the process is based on the heat cascade formulation in which all process heat requirements are represented by their temperature-enthalpy profiles that are corrected by minimum approach temperatures for a feasible heat exchange. This allows for determining the minimum energy requirement (MER) of the conversion process, from which appropriate technologies for the heat supply and mechanical energy recovery can be chosen. By considering the depleted and intermediate product streams as fuels for this purpose, the combined production of SNG, heat and power is then maximised by MILP, in which the material flows defined by the superstructure and the heat cascade act as constraints [22].
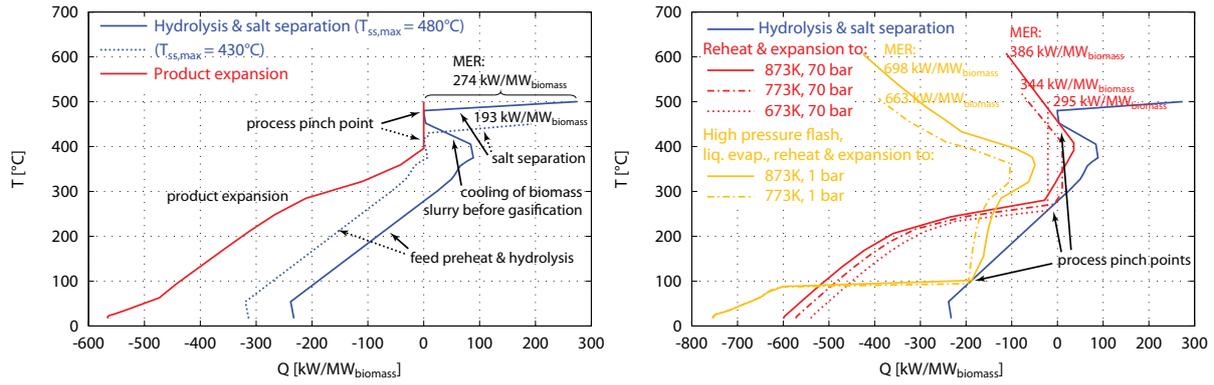
(a) Composite curves of the hot and cold process streams in the conversion units upstreams (blue) and downstreams (red/orange) of gasification
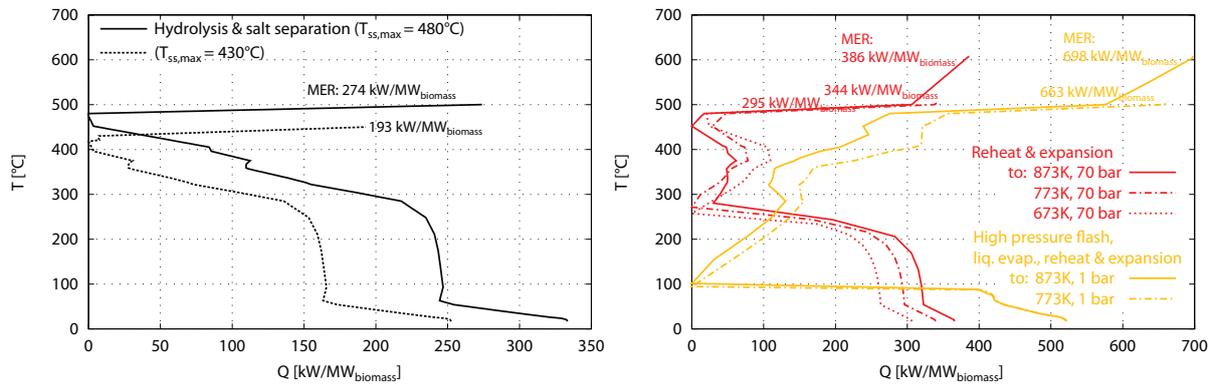
(b) Grand composite curves of all hot and cold process streams indicating the minimum energy requirements for heating and cooling

Figure 6: Process integration and minimum energy requirements (MER) on the composite curves for product expansion without power recovery (left) and for complete power recovery by reheating of entire condensable phase (right)

5.1 Minimum energy requirements

Figure 6 shows the minimum energy requirements of the principal flowsheeting options for wood at the default operating conditions of Table 3. The composite curves that identify the contributions of the process sections (Fig. 6(a)) highlight that the layout of the product separation and expansion section determines the pinch point and influences the energy demand markedly. If no power recovery from the crude product is performed (Fig. 6, left), the process pinch is situated at the salt separator and the MER is heavily dependent on the temperature to be reached. If $480°$C are required for a good precipitation of the diluted salts, the MER amounts to 274 kW $\mathrm{MW}_{biomass}^{-1}$ at $480°$C. If a maximum temperature of $430°$C in the separator is yet sufficient, only 193 kW $\mathrm{MW}_{biomass}^{-1}$ are needed at the pinch ($418°$C). Below, the specific and latent heat of the crude product is sufficient for preheating and hydrolysis of the feed, and an excess of 150-250 kW $\mathrm{MW}_{biomass}^{-1}$ can be recovered between 250 and $400°$C (Fig. 6(b)). Limited power recovery by liquid expansion of the high pressure condensate and/or expansion of the incondensable mixture with previous reheating to the process pinch does not change the MER and only marginally influences the amount of excess heat (not shown on figures).

If no separation at high pressure is applied and the crude product including the bulk water vapour is expanded in a turbine, the energy withdrawn as mechanical work is not available anymore at the gasification outlet temperature. As a consequence, the pinch point potentially shifts to the turbine outlet temperature and results in an increased MER at lower temperature (Fig. 6, right). Reheating the crude might thereby be required to avoid condensation in the final turbine stages and enhances the thermody-

Table 3: General assumptions and default operating conditions for Figure 6 and Table 5

Section	Operating conditions		Unit	Default
Feedstock	Type		-	wood
	Ash content		%wt$_{dry}$	0.6
	Composition (C, H, O, N)		%wt$_{daf}$	51.1, 5.8, 42.9, 0.2
Pretreatment	Total solids content of diluted feed		%wt	20
	Process pressure	p_{tot}	bar	300
Salt separation	Inlet temperature	$T_{ss,in}$	°C	350
	Maximum temperature	$T_{ss,max}$	°C	480
	Internal heat decrease	$\Delta T_{ss,int.}$	°C	20
	Outlet temperature	$\Delta T_{ss,out}$	°C	460
	ΔT at bottom	$\Delta T_{ss,bottom}$	°C	20
	ΔT at top	$\Delta T_{ss,top}$	°C	20
	Organic loss in salt brine		%	10
Gasification	Inlet temperature	$T_{g,in}$	°C	413
	Outlet temperature	$T_{g,out}$	°C	400
Water scrubber column	Bottom temperature		°C	30
	Pressure	$p_{hp,sep}$	bar	300
	Equilibrium stages	$N_{s,H2O}$	-	5
	CH$_4$ purity[a]	$\tilde{c}_{CH4,hp,out}$	%mol	94
Selexol column	CH$_4$ recovery	$r_{CH4,sel}$	%	98
	Absorption factor	A_{sel}	-	1.4
	CH$_4$ purity[a]	$\tilde{c}_{CH4,sel,out}$	%mol	94
SNG membrane	Material[a]	$y_{memb.}$	integer	2
Power recovery	Vapour phase	y^{v}_{prec}	integer	1
	Liquid phase	y^{l}_{prec}	integer	1
	Reheat temperature of vapour	$T_{g,s}$	°C	variable
Turbomachinery	Efficiency (isentropic)		%	80
Rankine cycle	Steam production pressure	$p_{s,p}$	bar	40/20[b]
	Steam superheat temperature	$T_{s,s}$	°C	350/270[b]
	Intermediate utilisation level	$T_{s,u}$	°C	200/120[b]
	Condensation level[c]		°C	19
	Efficiency, backpressure stages		%	80
	Efficiency, condensation stage		%	70
POX gas turbine	Pressure	p_{POX}	bar	14
	Fuel choice[d]	y_{fuel}	integer	1
	Additional steam per fuel i	$r_{fi,H2O}$	kg kg^{-1}	0.5
Energy integration	Fuel preheat temperature		°C	400
	Minimum approach temperatures	$\Delta T_{min}/2$	°C	8, 4, 2, 25
	(vapour & supercritical, liquid, phase-changing, reactive streams)			
NG grid specifications	CH$_4$ purity	$\tilde{c}_{CH4,grid}$	%	96
	Grid pressure	p_{grid}	bar	70

[a] For final SNG-upgrading with a polymeric membrane. Material choice (properties as in Gassner and Maréchal [18]): 1: cellulose acetate, 2: polysulfone

[b] with/without VL separation at high pressure

[c] Corresponds also to the low-temperature utilisation level

[d] Candidate fuels: 1: (crude) SNG, 2: recovered depleted stream from flash, 3: membrane permeate, combinations: 4: 1&2, 5: 1&3, 6: 2&3, 7: all.

namic conversion efficiency, which leads not only to an increased power output but also heat demand.

If the condensable phase from separation at high pressure is evaporated, reheated and expanded to atmospheric pressure, the characteristics of the process integration change drastically. For such a configuration, the pinch point shifts to the saturation temperature of the mixture at atmospheric pressure and the MER increases to 66-70% of the raw material's heating value. This would require to burn a large part of the produced gas and thus turn the generation of electrical power to the plant's main purpose.

5.2 Heat supply and cogeneration options

As mentioned earlier, the residual amount of methane and hydrogen in the depleted streams from the product separation may contribute to satisfy the process MER and reduce the amount of fuel to be withdrawn from the product stream in order to balance the heat demand. In the separation system superstructure of Figure 5, the waste streams considered for this purpose are the vapour phase recovered from flash drums at atmospheric pressure, the offgas from the Selexol regeneration column and the membrane permeate in the SNG postprocessing after bulk removal of CO_2. If these are not sufficient, crude SNG at grid pressure is identified as the appropriate stream to balance the heat requirement.

In addition to the embedded power generation from the exergy potential of the high pressure product, excess heat below the pinch can be recovered in a Rankine cycle to cogenerate electricity and industrial heat. In our model, the energy recovery potential of such a cycle is calculated with water as working fluid, although the temperature levels identified in Figure 6(b) suggest an organic fluid to be technically more relevant. Complementary to conventional waste heat recovery in a bottoming cycle, the pinch at a still moderate temperature level might also allow for high temperature cogeneration. Although gas engines or standard gas turbines are not adequate since the temperature level of the cogenerated heat is too low to efficiently balance the MER[12], less conventional gas turbine technology might yet be an option. One possibility is thereby not to limit the turbine inlet temperature by lean combustion, but to withdraw high temperature heat by radiative transfer from the combustion to satisfy the MER. Another option is to only partially oxidise the fuel in the gas turbine and complete the combustion after expansion. These options provide substantially more heat than standard gas turbines at the identified process pinch point, and internal heat recovery for air preheating and steam injection might further increase the cogeneration efficiency [14].

6 Process economics

6.1 Equipment rating and costing

The investment cost of a conceptual process design is estimated through rating and costing the major process equipment of Figure 1 that is required to reach the targeted conversion [20]. Following classic process design procedures [26, 43], the process vessels for reaction and separation are roughly sized for the specific operating conditions. Costing data from the same sources is then used to determine the investment required for the plant.

Before diluting and pressurisation, solid biomass feedstock has to be ground, whereas wet feedstock is dewatered in a sedimentation centrifuge. If sanitarily problematic waste biomass such as manure is used, the excess water is further purified by ultrafiltration and reverse osmosis, which also allows for recovering the nutrient salts and dissolved organic matter. The required membrane area for the unit has been reconciled with the available cost data [12, 43]. For the salt separator, the heat transfer area is determined in the energy-flow model and directly used for its costing as a shell-and-tube heat exchanger with a fixed tube sheet in titanium alloy. The gasification reactor is rated for a WHSV of 2 $kg_{biomass,daf}kg_{cat}^{-1}h^{-1}$ considering a dry catalyst bed density of 260 kg m^{-3}. The equipment for VL separation and gas absorption is sized according to design recommendations [43] assuming a tray efficiency of 15%. For CO_2 absorption in water at high pressure, the saturated solvent is simply expanded and flashed at atmospheric pressure to recover the residual fuel. The regeneration of Selexol requires a stripper of approximately equal size than the absorption tower. For the membrane stage, the same cost data as in Gassner and Maréchal [18] is used. The cost of combustion equipment is assessed with a correlation for alloy steel reformer furnaces [43]. For the heat exchanger network, the total heat transfer area and the minimum number of exchangers is estimated from the balanced composite curves following Ahmad et al. [44]. The cost of the network is assessed for fixed tube sheet heat exchangers of mixed carbon-steel/nickel-alloy construction at maximum process pressure with the averaged surface areas obtained for a reference heat transfer coefficient of 580 Wm^{-2}K^{-1} [14]. For all turbomachinery, centrifugal units are considered.

6.2 Running costs and plant profitability

The plant's operating costs C_{OP} for the conversion of one unit of biomass are calculated considering the expenses for the feedstock $C_{biomass}$, catalyst C_{cat}, utilities C_{UT}, operating labour C_{OL} and maintenance C_M (all in [$ MWh$_{biomass}^{-1}$]):

$$C_{OP} = C_{biomass} + C_{cat} + C_{UT} + C_{OL} + C_M \qquad (22)$$

$$\text{with:} \quad C_{UT} = \frac{\dot{E}^+}{\Delta h_{biomass}^0 \dot{m}_{biomass}^+} \cdot C_{el} \qquad (23)$$

$$C_{OL} = \frac{C_{salaries}}{t_a \cdot \Delta h_{biomass}^0 \dot{m}_{biomass}^+} \qquad (24)$$

$$C_M = 0.05 \cdot \frac{C_{GR}}{t_a \cdot \Delta h_{biomass}^0 \dot{m}_{biomass}^+} \qquad (25)$$

in which C_{el} corresponds to the electricity price, $C_{salaries}$ the employees' total yearly salaries, t_a the yearly operating time and C_{GR} the investment (grass roots) cost. In this formulation, the utility cost C_{UT} (Eq. 23) cancels out if the plant produces net electricity (i.e. $\dot{E}^+ = 0$, $\dot{E}^- > 0$), the maintenance cost C_M is supposed to amount to 5% of the investment per year and the catalyst cost C_{cat} is determined from its replacement rate $\dot{m}_{cat}$ with respect to the sulphur loading as calculated by Equations (20)-(21). Expressing the annualised investment as a depreciation cost $C_{GR,d}$ by discounting with the capital recovery factor at an interest rate i_r over the economic lifetime n of the plant, the total expenses C_{tot} [$ MWh$_{biomass}^{-1}$] are obtained by:

$$C_{tot} = C_{OP} + C_{GR,d} \qquad (26)$$

$$\text{with:} \quad C_{GR,d} = \frac{i_r(1+i_r)^n}{(1+i_r)^n - 1} \cdot \frac{C_{GR}}{t_a \cdot \Delta h_{biomass}^0 \dot{m}_{biomass}^+} \qquad (27)$$

Accounting for the earnings from selling SNG and the coproduced power and heat, the overall economic performance is expressed by the maximum acceptable biomass cost for the plant to break even $C_{biomass,be}$ [$ MWh$_{biomass}^{-1}$], i.e.:

$$C_{biomass,be} = C_{biomass,pr} + C_{biomass} \qquad (28)$$

$$C_{biomass,pr} = \varepsilon_{SNG} \cdot C_{SNG} + \varepsilon_{el} \cdot C_{el} + \varepsilon_{th} \cdot C_q - C_{tot} \qquad (29)$$

in which $C_{biomass,pr}$ represents the net profit obtained from the conversion of 1 MWh of biomass if SNG, electricity and heat are sold at prices of C_{SNG}, C_{el} and C_q, respectively.

The cost formulation of Equations (22)-(29) that is normalised with respect to the conversion of one unit of biomass provides a coherent assessment of the overall process economics. It is worthwhile to note that this would not be the case if the economic performance was based on the production cost for one unit of SNG, in which the benefits from selling the coproducts (heat and power) are accounted by negative contributions. Although convenient for a single product, such an assymetric assessement is misleading in a polygeneration context since it might suggest to enhance the coproduction of the (sold) by-products to the expense of the main one[14].

7 Results and Discussion

In order to illustrate the thermo-economic performance of the principal flowsheet alternatives and their impact on power cogeneration, Table 5 shows a screening of energy balances, efficiencies and costs for the conversion of wood at a plant scale of 20 MW$_{th,biomass}$ and the operating economic conditions of Table 3 and 4. The associated conceptual flowsheets are illustrated in Figure 7. Comparing the alternatives for product separation with a high pressure stage, the detailed electricity balance highlights the elevated pump power required for complete separation in a water scrubber column at 300 bar. Power recovery

Table 4: Economic assumptions

Parameter		Unit	Value
Wood price (Φ_{wood}=50%)	$C_{biomass}$	$\$ \, MWh^{-1}$	33
Electricity price (green)	C_{el}	$\$ \, MWh^{-1}$	180
SNG price	C_{SNG}	$\$ \, MWh^{-1}$	120
Catalyst price		$\$ \, kg^{-1}$	200
Operators		per shift[a]	4[b]
Operator salary		$\$ \, year^{-1}$	60'000
Maintenance cost		% of $C_{GR} \, year^{-1}$	5
Interest rate	i_r	%	6
Discount period	n	years	15
Yearly operating time	t_a	h	7690
Marshall & Swift index		-	1302[c]
Currency		US Dollars	

[a] Full time operation requires three shifts per day. With a working time of five days per week and 48 weeks per year, one operator per shift corresponds to 4.56 employees

[b] For a plant size of 20 $MW_{th,biomass}$. For other production scales, an exponent of 0.7 with respect to plant capacity is used

[c] Average of year 2006

through liquid expanders thus appears mandatory. From an efficiency point of view, bulk gas separation at grid pressure is still more competitive due to its lower power consumption. For both these options, the power recovery potential from expanding the vapour phase to grid pressure is relatively modest and only feasible at large production scales [14]. With bulk separation at high pressure, a Rankine cycle may generate 6-8% of the biomass input as electricity and allows for a positive net power balance. Due to the high marginal electric efficiency approaching 60%, the use of a partial oxidation turbine for high-temperature cogeneration might slightly increase the chemical efficiency-equivalent although the power potential is limited. If no separation at high pressure is applied and the entire crude product is reheated, expanded and separated at grid pressure, the product balance shifts towards an increased electricity generation to the expense of SNG. Both the product expansion turbine and the bottoming cycle generate substantially more power and integrate particularly well with a partial oxidation turbine. For all options, a substantial amount of energy is lost in form of the chemical potential of the substrate accompanying the salt brine withdrawn from the separator. The largest part of the energy loss is yet related to the heat evacuation by cold utility. If industrial heat can be used locally, increasing the condensation level of the Rankine cycle to 120°C for cogenerating heat in a distribution network at 110°C (70°C return) would eliminate the major part of this loss and increase the total energy efficiency ε to 77.1%, 77.7% and 81.2% for the three cases of Table 5 without partial oxidation turbines (i.e. VL and gas separation at high pressure, VL separation at high pressure and gas separation at grid pressure, and VL and gas separation at grid pressure, respectively). By recovering 19-28% of the biomass input as heat to the expense of a net decrease of the electricity yield by 3.0-4.6%, an equivalent coefficient of performance greater than 6 is thereby attained for the marginal substition of electricity by heat. Assuming a reference exergy efficiency of $\eta_{HP} = 55\%$ in the definition of ε_{chem} (Eq. 6) for this conversion by heat pumping [14], the polygeneration of fuel, heat and power allows for increasing the chemical efficiency of the configurations of Table 5 by 6-8 points.

The economic comparison assesses investment costs around 1'000 $ $kW_{biomass}^{-1}$ that increase with the share of cogenerated electricity. The total costs are dominated by the expenses for wood and would be considerably lowered if waste biomass was used. For the relatively small plant capacity reported here, the capital depreciation represents 17-20% of the total cost considering an interest rate of 6%. If the capital investment would be recovered at a 1.7 times higher recovery factor that corresponds to $i = 15\%$ and $n = 15$ years, the total cost would increase by 10-13% and require a similar increase of the revenues from selling SNG and power to maintain the same competitivity with respect to biomass break even cost. Depending on the process configuration, electricity cogeneration may thereby generate a considerable share of the total revenue, which makes the economically optimal plant design heavily dependent on the prevailing relative selling prices for renewable SNG and electricity. For the plant operation, the cost for

(a) Product separation by high pressure water absorption and a membrane at grid pressure

(b) Product separation by high pressure flash, selexol absorption and a membrane at grid pressure

(c) Expansion of the entire crude product and separation by selexol absorption and a membrane at grid pressure

Figure 7: Principal flowsheet options with energy balances and costs of Table 5 at default conditions of Table 3. Heat exchanger network, heat recovery system and utility system are not shown. Values in parenthesis correspond to configurations with a partial oxidation (POX) gas turbine

Table 5: Screening of energy balances, efficiencies and costs for the principal flowsheeting and power recovery options of Figure 5 for wood at the default operating conditions of Table 3

	High pressure separation Grid pressure gas separation Vapour reheat temperature $T_{g,s}$ POX turbine fuel		water absorption membrane 400 °C -	SNG	flash drum selexol abs. & memb. 400 °C -	crude SNG	- selexol abs. & memb. 600 °C -	crude SNG
Consumption	Biomass	kW	20'000	20'000	20'000	20'000	20'000	20'000
	Electricity							
	- process	kW	192	192	192	192	192	192
	- separation	kW	900	900	188	150	145	98
Production	SNG	kW	10'998	10'289	10'971	8'759	8'408	5'720
	Electricity							
	- vapour exp.	kW	169	146	386	336	1'933	1'809
	- liquid exp.	kW	627	627	92	92	21	21
	- POX turbine	kW	-	398	-	1'302	-	1'843
	- Rankine cycle	kW	1'362	1'396	1'297	1'252	1'533	1'368
	- net	kW	1'066	1'475	1'395	2'640	3'150	4'751
Losses	Total	kW	7'936	8'236	7'634	8'601	8'442	9'530
	- salt brine	kW	1'910	1'910	1'910	1'910	1'910	1'910
	- cooling water	kW	4'768	4'825	4'810	4'465	5'488	4'877
	- fumes	kW	552	573	557	699	759	927
	- latent heat[a]	kW	706	928	357	1'527	285	1'816
Efficiencies	ε_{SNG}	%	55.0	51.4	54.8	43.8	42.0	28.6
	ε_{el}	%	5.3	7.4	7.0	13.2	15.8	23.8
	ε	%	60.3	58.8	61.8	57.0	57.8	52.4
	η	%	55.4	53.9	56.7	52.1	52.7	47.5
	ε_{chem}	%	64.4	64.4	67.1	67.0	69.7	70.4
	$\Delta\varepsilon_{el,\,POX}$[b]	%	-	57.7	-	56.3	-	59.6
Economics	C_{GR}[c]	M$	17.9	19.0	19.4	21.4	20.8	22.6
	C_M	$ MWh$_{biomass}^{-1}$	5.8	6.2	6.3	7.0	6.8	7.3
	$C_{GR,d}$	$ MWh$_{biomass}^{-1}$	12.0	12.7	13.0	14.3	13.9	15.1
	C_{tot}[d]	$ MWh$_{biomass}^{-1}$	71.7	72.8	73.2	75.2	74.6	76.3
	$\varepsilon_{SNG}\cdot C_{SNG}$	$ MWh$_{biomass}^{-1}$	66.0	61.7	65.8	52.5	50.4	34.3
	$\varepsilon_{el}\cdot C_{el}$	$ MWh$_{biomass}^{-1}$	9.5	13.3	12.6	23.8	28.4	42.7
	$C_{biomass,pr}$	$ MWh$_{biomass}^{-1}$	3.8	2.2	5.2	1.1	4.2	0.7
	$C_{biomass,be}$	$ MWh$_{biomass}^{-1}$	36.8	35.2	38.2	34.1	37.2	33.7

[a] Difference in latent heat of the combustion products from biomass, SNG and on-site flue gas which is not accounted for in energy balances based on lower heating value. Calculated by difference.

[b] Defined as $\Delta\dot{E}/(\Delta h_{SNG}^0\Delta\dot{m}_{SNG})$ in comparison with the configuration without a partial oxidation gas turbine.

[c] Cost scaling exponents are in the range of 0.6-0.7 below 20 MW$_{th,biomass}$ and 0.8-0.9 above [19].

[d] At the selected operating conditions, plant scale and prices, C_{cat}, C_{OL} and $C_{biomass}$ contribute in all cases with 13.7, 7.2 and 33.0 $ MWh$_{biomass}^{-1}$, respectively.

catalyst replacement is important and severely limits the process efficiency. Other means than preventing catalyst deactivation by a high temperature in the salt separator to limit the dissolved sulphur content or an economic way for catalyst regeneration would thus be worthwile. As outlined in Section 5.1, a temperature reduction of 50°C in the salt separator decreases the MER by 30% and would thus allow for a higher product yield since less fuel needs to be withdrawn for heat supply.

Table 6 compares the projected process efficiency of hydrothermal gasification with the major competing routes for the polygeneration of fuels, power and heat from lignocellulosic biomass. These data have been obtained using a similar methodology based on the same assumptions and level of detail. Even at an initial moisture content of 50%, the conversion in supercritical water outperforms the fermentation of ethanol [45] and the thermochemical production of liquid fuels[46], and is on a par with the one of SNG by conventional biomass gasification and methanation. However, processing biomass at 80% instead of 50% moisture with conventional technology would require to evaporate an additional amount

Table 6: Projected energy efficiencies of the major competing technologies for the polygeneration of fuels, heat and power from lignocellulosic biomass (at 50% moisture, values in % according to Eqns. (1)-(6), all without optimisation)

Type	ε_{fuel}	ε_{el}	ε_{th}	ε_{chem}
without heat cogeneration				
- Methanol [46]	57	-6	-	47
- Dimethyl ether [46]	56	-5	-	48
- Fischer-Tropsch (crude) [46]	60	-0.4	-	59
- Ethanol [45, 47]	32	18	-	62
- Ethanol & SNG (conv.) [47]	74	-0.5	-	79
- SNG, conventional gas.[18, 48]	61	5	-	71
	74	2	-	77
- SNG, hydrothermal gas.	55	7	-	67
	29	24	-	70
with heat cogeneration				
- SNG, conventional gas.[18, 48]	61	5	9	73
	74	0.1	8	78
- hydrothermal gasification	55	4	19	73
	29	20	25	77

of 3 kg of water per kg of dry matter, whose total enthalpy of vaporisation corresponds to 39% of the biomass' lower heating value. Even if done in multiple effects, this represents a severe energy penalty and demonstrates the advantage of the hydrothermal route for wet substrates.

8   Conclusions

This paper has presented a systematic analysis of the process design and integration alternatives for SNG production by hydrothermal gasification of wet biomass in supercritical water. For this purpose, thermo-economic models for promising candidate technologies have been developed, reconciled and validated with data from experimental investigations and process demonstration. A general superstructure for combined product separation and internal energy recovery from the supercritical conditions has been established to explore the possibilities for an efficient cogeneration of SNG and power. Simultaneously considering the mass and energy balances in the process integration thereby allows for linking the synthesis of the separation and energy recovery systems while considering the depleted streams as fuels to balance the heat demand of the process.

With conservative hypotheses on practical design limitations such as a maximum total solids content of 20% in the feed and the loss of 10% of the hydrolysate in the salt slurry, the preliminary results show that a sound process integration and energy recovery allows for an energetically and economically viable process. The design is thereby very flexible in terms of the relative SNG and electricity yields that can be adjusted to expected market prices of these services. Catalyst deactivation is further identified as a bottleneck for the process design since it may require to operate at relatively unefficient conditions. These thermodynamic and thermo-economic trade-offs are systematically explored by optimisation in an associated paper [19].

Acknowledgements

References

[1] Y. Matsumura, T. Minowa, B. Potic, S. R. A. Kersten, W. Prins, W. P. M. Van Swaaij, B. Van De Beld, D. C. Elliott, G. G. Neuenschwander, A. Kruse, and M. J. Antal Jr. Biomass gasification in near- and super-critical water: Status and prospects. *Biomass and Bioenergy*, 29(4):269–292, 2005.

[2] A. Kruse. Supercritical water gasification. *Biofuels, Bioproducts and Biorefining*, 2(5):415–437, 2008.

[3] A. Kruse. Hydrothermal biomass gasification. *Journal of Supercritical Fluids*, 47(3):391–399, 2009.

[4] D. C. Elliott. Catalytic hydrothermal gasification of biomass. *Biofuels, Bioproducts and Biorefining*, 2(3):254–265, 2008.

[5] Andrew A. Peterson, Frédéric Vogel, Russell P. Lachance, Morgan Fröling, Michael J. Antal Jr., and Jefferson W. Tester. Thermochemical biofuel production in hydrothermal media: A review of sub- and supercritical water technologies. *Energy and Environmental Science*, 1(1):32–65, 2008.

[6] F. Vogel, M. H. Waldner, A. A. Rouff, and S. Rabe. Synthetic natural gas from biomass by catalytic conversion in supercritical water. *Green Chemistry*, 9(6):616–619, 2007.

[7] Maurice H. Waldner and Frédéric Vogel. Renewable production of methane from woody biomass by catalytic hydrothermal gasification. *Industrial and Engineering Chemistry Research*, 44:4543–4551, 2005.

[8] A. A. Peterson, P. Vontobel, F. Vogel, and J. W. Tester. In situ visualization of the performance of a supercritical-water salt separator using neutron radiography. *Journal of Supercritical Fluids*, 43 (3):490–499, 2008.

[9] A. A. Peterson, P. Vontobel, F. Vogel, and J. W. Tester. Normal-phase dynamic imaging of supercritical-water salt precipitation using neutron radiography. *Journal of Supercritical Fluids*, 49(1):71–78, 2009.

[10] Martin Schubert, Johann W. Regler, and Frédéric Vogel. Continuous salt precipitation and separation from supercritical water. Part 1: Type 1 salts. *Journal of Supercritical Fluids*, 52:99–112, 2010.

[11] Martin Schubert, Johann W. Regler, and Frédéric Vogel. Continuous salt precipitation and separation from supercritical water. Part 2: Type 2 salts and mixture of two salts. *Journal of Supercritical Fluids*, 52:113–124, 2010.

[12] J. Luterbacher, M. Fröling, F. Vogel, F. Maréchal, and J. W. Tester. Hydrothermal gasification of waste biomass: Process design and life cycle assessment. *Environmental Science and Technology*, 43:1578–1583, 2009.

[13] M. Naqvi, J. Yan, and M. Fröling. Bio-refinery system of DME or CH_4 production from black liquor gasification in pulp mills. *Bioresource technology*, 101(3):937–944, 2010.

[14] Martin Gassner. *Process design methodology for thermochemical production of fuels from biomass. Application to the production of Synthetic Natural Gas from lignocellulosic resources*. PhD thesis, EPFL, 2010. doi: 10.5075/epfl-thesis-4693.

[15] Anne-Laure Cuvilliez, Jeremy S. Luterbacher, Martin Gassner, François Maréchal, and Larry P. Walker. Process design and life cycle analysis of a lignocellulosic bioethanol process: Comparing pretreatment options. In *23th International conference on efficiency, cost, optimization, simulation and environmental impact of energy systems (ECOS)*, 2010.

[16] A. G. Haiduc, M. Brandenberger, S. Suquet, F. Vogel, R. Bernier-Latmani, and C. Ludwig. SunCHem: An integrated process for the hydrothermal production of methane from microalgae and CO_2 mitigation. *Journal of Applied Phycology*, 21(5):529–541, 2009.

[17] S. Stucki, F. Vogel, C. Ludwig, A. G. Haiduc, and M. Brandenberger. Catalytic gasification of algae in supercritical water for biofuel production and carbon capture. *Energy and Environmental Science*, 2(5):535–541, 2009.

[18] Martin Gassner and François Maréchal. Thermo-economic process model for thermochemical production of Synthetic Natural Gas (SNG) from lignocellulosic biomass. *Biomass and Bioenergy*, 33: 1587–1604, 2009. doi: 10.1016/j.biombioe.2009.08.004.

[19] Martin Gassner, Frédéric Vogel, Georges Heyen, and François Maréchal. Optimal process design for the polygeneration of SNG, power and heat by hydrothermal gasification of waste biomass: Process optimisation for selected substrates. *Energy and Environmental Science*, page in press, 2011. doi: 10.1039/C0EE00634C.

[20] Martin Gassner and François Maréchal. Methodology for the optimal thermo-economic, multi-objective design of thermochemical fuel production from biomass. *Computers and Chemical Engineering*, 33:769–781, 2009.

[21] Belsim SA. Vali IV. www.belsim.com, last visited 04/2009.

[22] Martin Gassner and François Maréchal. Combined mass and energy integration in process design at the example of membrane-based gas separation systems. *Computers and Chemical Engineering*, 34(12):2033–2042, 2010. Invited publication for the special edition of PSE 2009.

[23] Werner Boie. Fuel technology calculations. *Energietechnik*, 3:309–316, 1953.

[24] J. Szargut and T. Styrylska. Angenäherte Bestimmung der Exergie von Brennstoffen. *Brennstoff-Wärme-Kraft*, 16:589–636, 1964.

[25] D. Favrat, F. Marechal, and O. Epelly. The challenge of introducing an exergy indicator in a local law on energy. *Energy*, 33(2):130–136, 2008.

[26] R. Turton, R. C. Bailie, W. B. Whiting, and J. A. Shaeiwitz. *Analysis, synthesis, and design of chemical processes*. Prentice Hall, New York, 1998.

[27] Martin Gassner and François Maréchal. Thermodynamic comparison of the FICFB and Viking gasification concepts. *Energy*, 34:1744–1753, 2009. doi: 10.1016/j.energy.2009.05.011. Invited publication for the special edition of PRES 2008.

[28] SVGW. G13, Richtlinien für die Einspeisung von Biogas ins Erdgasnetz. Zürich, Switzerland, 2008.

[29] Martin Gassner, Renato Baciocchi, François Maréchal, and Marco Mazzotti. Integrated design of a gas separation system for the upgrade of crude SNG with membranes. *Chemical Engineering and Processing: Process Intensification*, 48:1391–1404, 2009.

[30] D. Peng and D. B. Robinson. A new two-constant equation of state. *Industrial and Engineering Chemistry Fundamentals*, 15(1):59–64, 1976.

[31] Byung I. Lee and Michael G. Kesler. Generalized thermodynamic correlation based on three-parameter corresponding states. *AIChE Journal*, 21(3):510–527, 1975.

[32] Z. Duan, N. Møller, and J. H. Weare. An equation of state for the CH_4-CO_2-H_2O system: I. Pure systems from 0 to 1000°C and 0 to 8000 bar. *Geochimica et Cosmochimica Acta*, 56:2605–2617, 1992.

[33] Z. Duan, N. Møller, and J. H. Weare. An equation of state for the CH_4-CO_2-H_2O system: II. Mixtures from 50 to 1000°C and 0 to 1000 bar. *Geochimica et Cosmochimica Acta*, 56:2619–2631, 1992.

[34] Gregory Esser and Georges Heyen. Étude thermodynamique d'un procédé de gazéification de biomass à pression élevée. Master's thesis, Université de Liège, 2008.

[35] Z. Duan and R. Sun. An improved model calculating CO_2 solubility in pure water and aqueous NaCl solutions from 273 to 533 K and from 0 to 2000 bar. *Chemical Geology*, 193:257–271, 2003.

[36] Z. Duan and S. Mao. A thermodynamic model for calculating methane solubility, density and gas phase composition of methane-bearing aqueous fluids from 273 to 523 K and from 1 to 2000 bar. *Geochimica et Cosmochimica Acta*, 70:3369–3386, 2006.

[37] J. Qin, R. J. Rosenbauer, and Z. Duan. Experimental measurements of vapor-liquid equilibria of the CH_4-CO_2-H_2O ternary system. *Journal of Chemical and Engineering Data*, 53:1246–1249, 2008.

[38] ECN. Phyllis, database for biomass and waste. www.ecn.nl/phyllis, last visited 06/2009.

[39] Ingo Leusbrock, Sybrand J. Metz, Glenn Rexwinkel, and Geert F. Versteeg. Quantitative approaches for the description of solubilities of inorganic compounds in near-critical and supercritical water. *Journal of Supercritical Fluids*, 47:117–127, 2008.

[40] F. Vogel, M. H. Waldner, T.-B. Truong, E. De Boni, and S. Stucki. Verfahren zur Erzeugung von Methan und Methanhydrat aus Biomasse (Process for the production of methane and methane hydrate from biomass). Paul Scherrer Institut, Patent application PCT 05021601.9/EP 05022101 (2005-10-04), 2005.

[41] M. J. Perlmutter, H. E. Kimmel, C. Chiu, and H. Paradowski. Economic and environmental benefits of two-phase LNG expanders. In *14th International conference & exhibition on liquefied natural gas (LNG14)*, pages 1121–1130, Doha, Qatar, March 21-24 2004.

[42] A. Y. Houde, B. Krishnakumar, S. G. Charati, and S. A. Stern. Permeability of dense (homogeneous) cellulose acetate membranes to methane, carbon dioxide, and their mixtures at elevated pressures. *Journal of Applied Polymer Science*, 62(13):2181–2192, 1996.

[43] G. D. Ulrich and P. T. Vasudevan. *Chemical engineering process design and economics. A practical guide*. Process publishing, New Hampshire, 2nd edition, 2004.

[44] S. Ahmad, B. Linnhoff, and R. Smith. Cost optimum heat exchanger networks – 2. Targets and design for detailed capital cost models. *Computers and Chemical Engineering*, 14(7):757–767, 1990.

[45] Suping Zhang, François Maréchal, Martin Gassner, Zoé Périn-Levasseur, Wei Qi, Zhengwei Ren, Yongjie Yan, and Daniel Favrat. Process modeling and integration of fuel ethanol production from lignocellulosic biomass based on double acid hydrolysis. *Energy and Fuels*, 23:1759–1765, 2009.

[46] Laurence Tock, Martin Gassner, and François Maréchal. Thermo-economic process model for thermochemical production of liquid fuels from lignocellulosic biomass. *Biomass and Bioenergy*, 34:1838–1854, 2010.

[47] Martin Gassner and François Maréchal. Increasing Conversion Efficiency in Fuel Ethanol Production from Lignocellulosic Biomass by Polygeneration - and a Paradoxon between Energy and Exergy in Process Integration. In *23th International conference on efficiency, cost, optimization, simulation and environmental impact of energy systems (ECOS)*, 2010.

[48] S. Heyne, H. Thunman, and S. Harvey. Extending existing CHP plants for SNG production – a process integration study. *International Journal of Energy Research*, page submitted, 2010.